ARCHIVES of FOUNDRY ENGINEERING

Published quarterly as the organ of the Foundry Commission of the Polish Academy of Sciences

ISSN (1897-3310)
Volume 8
Special Issue
3/2008

39 – 44

9/3

Influence of coolant motion on structure of hardened steel element

A. Kulawik[a], T. Skrzypczak[a,*] E. Węgrzyn-Skrzypczak [b]

[a] Institute of Mechanics and Machine Design, Technical University of Częstochowa, st. Dąbrowskiego 73, 42-200 Częstochowa, Poland

[b] Institute of Mathematics and Computer Science, Technical University of Częstochowa, st. Dąbrowskiego 73, 42-200 Częstochowa, Poland

*Corresponding author. E-mail address: skrzyp@imipkm.pcz.czest.pl

Received 01.07.2008; accepted in revised form 17.07.2008

Abstract

Presented paper is focused on volumetric hardening process using liquid low melting point metal as a coolant. Effect of convective motion of the coolant on material structure after hardening is investigated. Comparison with results obtained for model neglecting motion of liquid is executed. Mathematical and numerical model based on Finite Element Metod is described. Characteristic Based Split (CBS) method is used to uncouple velocities and pressure and finally to solve Navier-Stokes equation. Petrov-Galerkin formulation is employed to stabilize convective term in heat transport equation. Phase transformations model is created on the basis of Johnson-Mehl and Avrami laws. Continuous cooling diagram (CTPc) for C45 steel is exploited in presented model of phase transformations. Temporary temperatures, phases participation, thermal and structural strains in hardening element and coolant velocities are shown and discussed.

Keywords: Heat Treatment; Phase Transformations; Natural Convection; Finite Element Method

1. Introduction

There are many variables which affects hardening process. Most of them are deciding factors i.e., sort, temperature and material properties of cooling medium, adopted cooling metod, shape of the hardening part etc. Variety of mentioned parameters prompt technologists to search for solutions which shows transformations occuring during hardening process on the desired level of accuracy. Various mathematical and numerical models are exploited to solve such formulated problems. In these models effect of convective motion of cooling medium i.e., air, water, oil etc., on cooling rate of hardening element is mostly neglected. Construction of the geometry and spatial discretization of collant filled region is often not executed. Instead of that appropriate boundary conditions are introduced to assure heat receiving from hardening part.

In presented paper region filled with liquid metallic medium is introduced and spatially discretized. Thermally induced convective motion of the coolant is considered. Influence of this phenomenon on heat exchange between coolant and steel part is investigated. High temperature gradients in the vicinity of cooling element cause intensive motion of the liquid metallic material. High rate of liquid motion near boundaries has significant effect on the heat transport. Such formulation of the steel hardening process and application of liquid metal as cooling medium is unusual in literature and deserves consideration.

2. Mathematical model

Considered region (fig. 1) contains two subregions – hardening element Ω_S and liquid coolant Ω_L. Heat from the coolant is transfered outside boundary Γ_L with using of appropriate boundary condition. In the beginning of the process steel element has constant initial temperature higher than austenitic transformation temperature. Initial temperature of the coolant is set slightly above its melting point. Preliminary liquid movements triggered by putting the element into coolant are neglected.

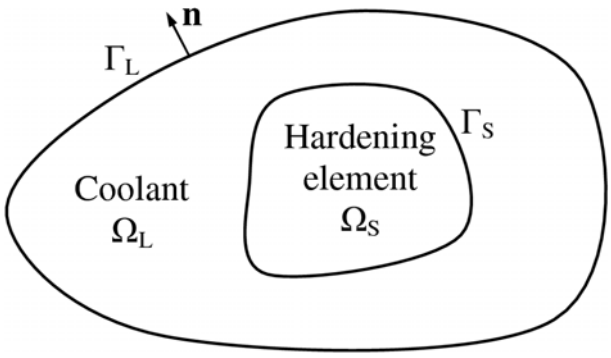

Fig. 1. Considered region consists of hardening element Ω_S and coolant Ω_L

The base of mathematical model consists of partial differential equations of momentum, continuity and heat transport with convective term [1]. This set is completed by eqations of the kinetics of phase transformations.

$$c\rho\left(\frac{\partial T}{\partial t}+u_i T_{,i}\right)=\left(\lambda T_{,i}\right)_{,i} \tag{1}$$

$$\frac{\mu}{\rho}u_{i,jj}-u_j u_{i,j}-\frac{1}{\rho}p_{,i}-g_i\beta(T-T_{ref})=\frac{\partial u_i}{\partial t} \tag{2}$$

$$u_{i,i}=0 \tag{3}$$

where: T [K] denotes temperature, u_i [m/s] - velocity component int the ith-direction, t [s] - time, λ [W/m^{2}K] – thermal conductivity coefficient, μ [kg/ms] – dynamic viscosity, ρ [kg/m^3] - density, g_i [m/s^2] – acceleration component in the ith-direction, β [K^{-1}] – volumetric thermal expansion coefficient, T_{ref} [K] – reference temperature.

Equations (1-3) are completed by appropriate boundary conditions:

$$\mathbf{x}\in\Gamma_L:-\lambda\ \mathbf{n}\cdot\mathbf{grad}T=\alpha(T-T_\infty),\quad \mathbf{x}\in\Gamma_{L,S}:u_i=0 \tag{4}$$

and initial conditions:

$$t=0:T\big|_{\Omega_L}=T_L,\quad T\big|_{\Omega_S}=T_S,\quad u_i=0 \tag{5}$$

where: α [W/m^{2}K] is heat convection coefficient, T_∞ [K] – ambient temperature, T_S, T_L [K] – initial temperature of the hardening element and coolant respectively, $\mathbf{n}$ – vector outward normal to the external boundary Γ_L.

Continuous cooling diagram for C45 steel is used in presented phase transformations model [2]. Temporary values of temperature, time and maximum participation of the particular phase in the current cooling cycle are obtained from them. Kinetics of the ith-phase is calculated from empiric Avrami equation for cooling process [3-5]:

$$\eta_{(i)}(T,t)=\min\left\{\eta_{(i\%)},\widetilde{\eta}_\gamma-\sum_{j\neq i}\eta_j\right\}\cdot\left(1-\exp\left(-b(T)t^{n(T)}\right)\right) \tag{6}$$

where: $\widetilde{\eta}_\gamma$ denotes volumetric participation of the austenite, η_j is volumetric participation of the phases created during cooling process, $\eta_{(i\%)}$ is final participation of the ith-phase estimated from the CTPc diagram, $b(T)$ and $n(T)$ are temperature and time (t_S, t_f) of the beginning and end of phase transformation dependent coefficients.

Kinetics of the phases growth is continuous in presented solid state phase transformations model. Special function defined piecewise by kinetics function of the phases is introduced. Coefficients occuring in these functions are obtained from CTPc diagram. Three variants of phase kinetics are considered according to informations about creation of particular phase.

If maximum value of participation of the particular phase and final time of its creation is predicted, the begining of phase transformation will be calculated from following equation [4,5]:

$$t_s(t,\eta_\%,t_f)=\left(\frac{t^{\frac{A}{B(\eta_\%)}}}{t_f}\right)^{\left(\frac{B(\eta_\%)}{A-B(\eta_\%)}\right)} \tag{7}$$

If the end of first transformation, its maximum participation and starting time of the transformations is known, ending of the transformations will be estimated from below relation [4,5]:

$$t_f(t,\eta_\%,t_s)=\exp\left(\frac{-A\cdot(\ln(t_s)-\ln(t))}{B(\eta_\%)}\right)\cdot t_s \tag{8}$$

where: $\eta_\%$ is predicted volumetric participation of the phase.

In case of phase transformation occuring between others transformations, start and end of them are calculated from following equation [4,5]:

$$t_s\left(t_1,\eta_{(1\%)},t_2,\eta_{(2\%)}\right)=$$
$$=N\left(\eta_{(1\%)},\eta_{(2\%)}\right)\sqrt{\left(\frac{t_1^{\frac{B\left(\eta_{(1\%)}\right)}{A}}}{\exp\left(-\frac{A}{B\left(\eta_{(2\%)}\right)}\cdot\ln\left(t_2\right)\right)}\right)^{\frac{\mathrm{B}\left(\eta_{(1\%)}\right)}{A-\mathrm{B}\left(\eta_{(1\%)}\right)}}} \tag{9}$$

where: A, B and N coefficients are evaluated from relation:

$$N\left(\eta_{(1\%)},\eta_{(2\%)}\right)=\left(\frac{-A}{\mathrm{B}\left(\eta_{(2\%)}\right)}+1\right)\left(\frac{\mathrm{B}\left(\eta_{(1\%)}\right)}{A-\mathrm{B}\left(\eta_{(1\%)}\right)}\right)+1 \tag{10}$$

$$A=\exp\left(\ln\left(\frac{\ln\left(1-\eta_f\right)}{\ln\left(1-\eta_s\right)}\right)\right),\quad B\left(\eta_{\%}\right)=\ln\left(\frac{\ln\left(1-\eta_{\%}\right)}{\ln\left(1-\eta_s\right)}\right) \tag{11}$$

Participation of created martensite is evaluated on the base of empiric Koistinen-Marburger equation [6]:

$$\eta_M\left(T,t\right)=\left(\tilde{\eta}_A-\sum_{\alpha\neq M}\eta_\alpha\right)\left(1-\exp\left(-k\left(M_S-T\right)\right)\right),\ k=$$
$$=-\ln\left(\sum_\alpha\eta_\alpha\right)/\left(M_s-M_f\right) \tag{12}$$

where: M_s denotes initial temperature of the martensitic transformation estimated on the base of CTPc diagram.

Increment of the temperature and phase transformations dependent strain $d\varepsilon^{Tph}=d\varepsilon^{T}+d\varepsilon^{ph}$ are obtained from following relation:

$$d\varepsilon^{T}=\sum_i\alpha_i\left(T\right)\eta_i dT,\quad d\varepsilon^{ph}=\sum_i\gamma_i\left(T\right)d\eta_i \tag{13}$$

where: α_i is linear thermal expansion coefficient of the ith-phase, $\gamma_i=\delta V_i/\left(3V\right)$ denotes coefficient of volume change during ith-phase transformation.

2. Numerical model

The weighted residual method [7] for the heat transport equation (1) is adopted. Equation is multiplied by weighting function w and integrated over domain Ω_L and Ω_S:

$$\int_{\Omega_{L,S}}w\left[\left(\lambda T_{,i}\right)_{,i}-c\rho\left(T\right)\left(\frac{\partial T}{\partial t}+u_iT_{,i}\right)\right]d\Omega_{L,S}=0 \tag{14}$$

Above equation is written in weak form:

$$\int_{\Omega_{L,S}}\lambda w_{,i}\,T_{,i}\,d\Omega+\int_{\Omega_{L,S}}c\rho wu_iT_{,i}\,d\Omega+\int_{\Omega_{L,S}}c\rho w\frac{\partial T}{\partial t}d\Omega=$$
$$=\oint_{\Gamma_L}wq_nd\Gamma_L \tag{15}$$

Weak form of (14) is discretized over space with using of Petrov-Galerkin method [8-11]. After time discretization procedure (Euler backward scheme) in relation to time derivative occuring in (15) and agregation of the discrete model global finite element equation is obtained

$$\left(\mathbf{K}+\mathbf{A}+\frac{1}{\Delta t}\mathbf{M}\right)\mathbf{T}^{f+1}=\frac{1}{\Delta t}\mathbf{M}\mathbf{T}^{f}+\mathbf{B} \tag{16}$$

where: **K** is heat conductivity matrix, **A** – heat advection matrix, **M -** heat capacity matrix and **B -** right hand side vector.

Momentum equation (2) is solved only in region Ω_L filled with coolant with using Characteristic Based Split (CBS) scheme. CBS is based on the projection method developed by Chorin [12] and described by Zienkiewicz and Codina [13] and Zienkiewicz and Taylor [14]. In this method an auxiliary velocity field $\mathbf{u}^*$ is introduced [15] to uncouple equations (2) and (3):

$$\Delta u_i^*=u_i^*-u_i^f=\Delta t\left[\frac{\mu}{\rho}u_{i,jj}-u_ju_{i,j}-g_i\beta(T-T_{ref})+\right.$$
$$\left.+\frac{\Delta t}{2}u_k\left[u_ju_{i,j}+g_i\beta\left(T-T_{ref}\right)\right]_{,k}\right]_{t=t^f} \tag{17}$$

The final velocity field is corrected by the pressure increment so that is divergence free:

$$u_i^{f+1}-u_i^*=-\frac{\Delta t}{\rho}\left(p_{,i}\right)^{f+1} \tag{18}$$

By taking the divergence of (22) the following Poisson equation for the pressure is obtained:

$$\Delta t\left(p_{,ii}\right)^{f+1}=\rho u_{i}^{*}{}_{,i} \tag{19}$$

Standard Galerkin procedure is then applied for equations (17-19).

3. Examples of calculation

Geometry of the hardening part Ω_S surrounded by cooling liquid Ω_L is presented in fig. 2. Effect of coolant motion on distribution of ferrite, perlite and bainite was investigated.

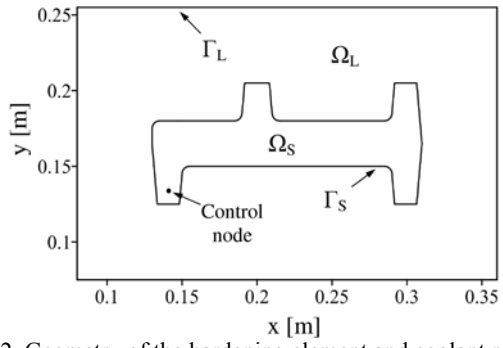

Fig. 2. Geometry of the hardening element and coolant region used in calculation. Control node is marked with black dot.

Following boundary and initial conditions were introduced for heat transport equation

- Newton boundary condition on external boundary Γ_L with $\alpha=1000$ [W/m^{2}K], $T_\infty=375$ [K];
- ideal contact between hardening element and coolant on internal boundary Γ_S;
- initial temperature of hardening element was equal to $T_S=1100$ [K], initial temperature of coolant $T_L=375$ [K];

Navier-Stokes equation was completed by following boundary and initial conditions

- Dirichlet boundary condition on boundaries Γ_L and Γ_S with $u_i=0$;
- initial velocities in coolant $u_i=0$ [m/s].

CTPc diagram for austenitization temperature *1153* [K] [2] was used in calculations on account of initial temperature level. Material properties used in calculations are collected in tables 1-2.

Table 1.
Material properties of hardening element and coolant

Material property	Hardening element	Coolant
λ	*48*	*68*
c	*481*	*1045*
ρ	*7760*	*852*
μ	-	*0.000264*
β	-	*0.000271*

Table 2.
Thermal and structural expansion coefficients [5]

Phase	α_i [1/K]	γ_i
Austenite	$2{,}178\times10^{-5}$	$1{,}986\times10^{-3}$
Ferrite	$1{,}534\times10^{-5}$	$1{,}534\times10^{-3}$
Pearlite	$1{,}534\times10^{-5}$	$1{,}534\times10^{-3}$
Bainite	$1{,}171\times10^{-5}$	$4{,}0\times10^{-3}$
Martensite	$1{,}36\times10^{-5}$	$6{,}5\times10^{-3}$

In the fig. 3-5 participation of ferrite, pearlite and bainite after hardening process are presented. Thermal and structural strains are shown in fig. 6. Results obtained for both variants of simulation are compared.

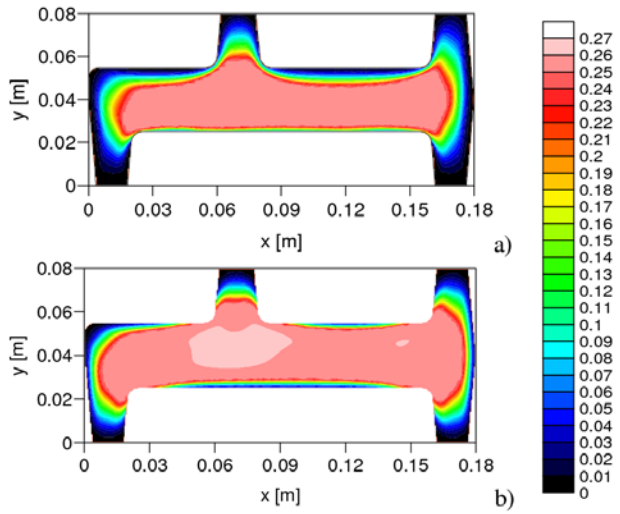

Fig. 3. Participation of ferrite after finishing a cooling process with coolant motion a) and without coolant motion b)

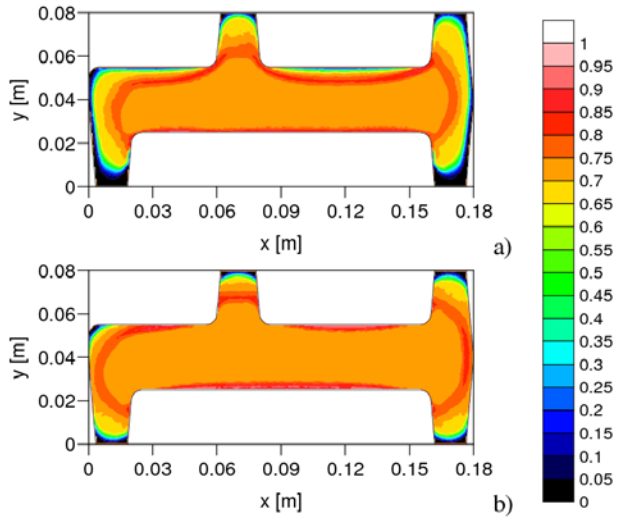

Fig. 4. Participation of pearlite after finishing a cooling process with coolant motion a) and without coolant motion b)

Significant differences in spatial distribution of ferrite, pearlite and bainite in case of considering coolant motion during hardening process in comparison with variant neglecting velocities are noticed. Cooling rates during early stage of process are definitely higher if motion of the liquid is taken into account. It results from intensive mixing of hot and cold material according to temperature gradients.

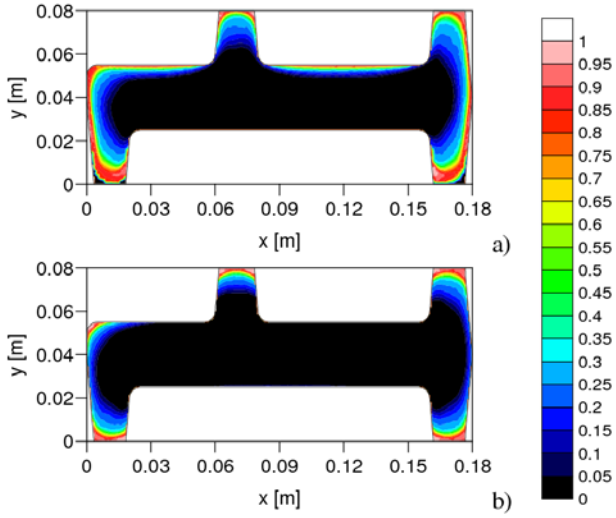

Fig. 5. Participation of bainite after finishing a cooling process with coolant motion a) and without coolant motion b)

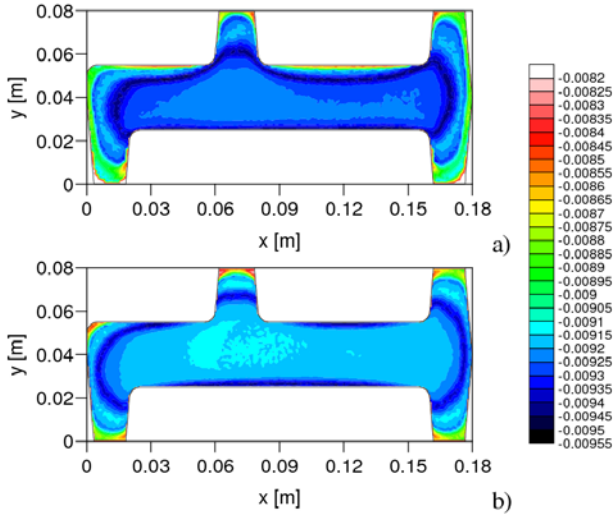

Fig. 6. Thermal and structural strains after finishing a cooling process with coolant motion a) and without coolant motion b)

High cooling rates during early stage of hardening process favors deeper hardened region evolution which provides bainite spatial distribution presented in fig. 5a. Depth of high bainite concentration zone is different on the upper and lower boundary of steel element according to rate of convective motion of the coolant. Hardened layer penetrates deeper the upper boundary because of intensive cooling. Bainite vanishes on the lower boundary where convection is weak. Neglecting coolant motion causes lower concentration of bainite on the upper boundary of hardened element.

In the fig. 7a-b velocities in the coolant after *15* and *700* [s] are presented. Initially strong convective cells in the upper part of liquid region are noticed. In the lower part liquid remains almost steady. After few minutes velocities in whole liquid become comparable.

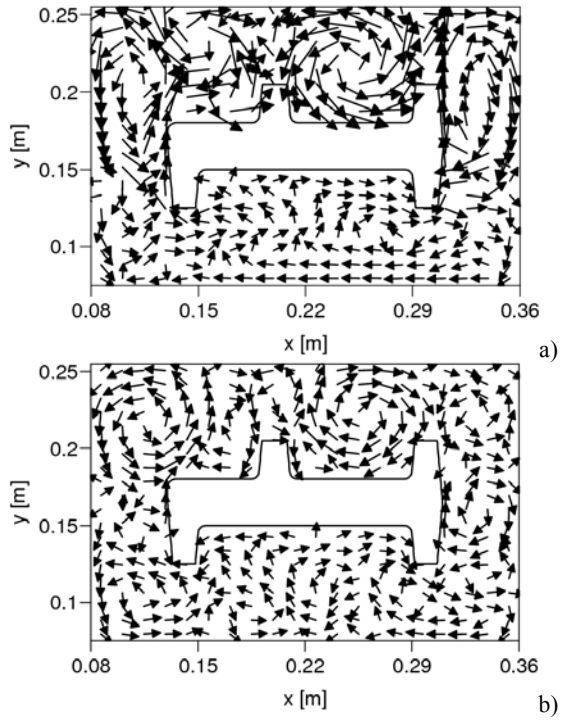

Fig. 7. Coolant motion during early stage a) and near the end of process

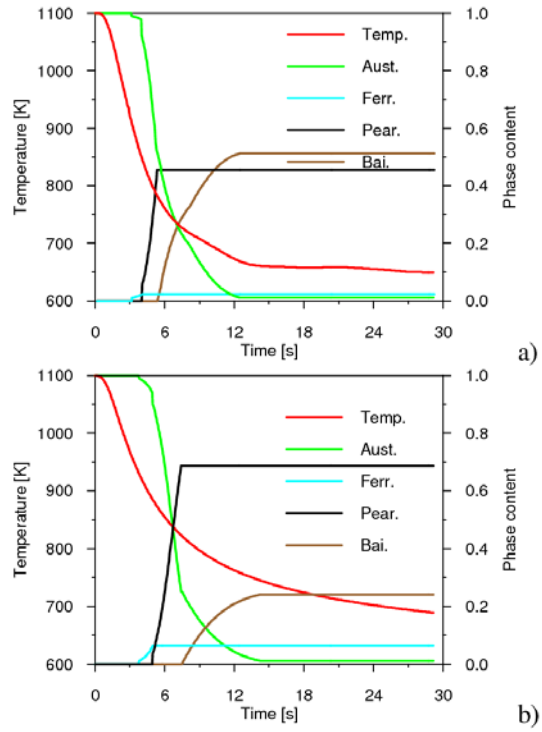

Fig. 8. Changes of participation of phases in control node according to time in case of moving coolant a) and without coolant movement b)

Changes of the phases participation according to time are presented in diagrams 8a-b. In the control node concentration of bainite is greater than *0.5* in first variant of simulation while second one gives result about *0.25*. It proves significant effect of coolant motion on hardening process.

4. Conclusions

Presented model may be used to estimate of kinetics and distribution of phases in the solid state, after solidification process. It may be adopted to optimization of heat treatment processes to obtain appropriate structure and hardness of steel during precise cooling process.

References

[1] E. Węgrzyn-Skrzypczak, Modelling of solidification with motion of the fluid in liquid and mushy zone, PhD Thesis, Częstochowa 2005 (in Polish).

[2] J. Orlich, A. Rose, P. Wiest, Atlas zur Wärmebehandlung von Stähle, III Zeit Temperatur Austenitisierung Schaubilder, Verlag Stahleisen MBH, vol 1 (1973).

[3] M. J. Avrami, Chem. Phys. 7, 1939.

[4] A. Bokota, A. Kulawik, Model and numerical analysis of hardening process phenomena for medium-carbon steel, Archives of Metallurgy and Materials, vol. 52 (2007) 337-346.

[5] A. Kulawik, Numerical analysis of thermal and mechanical phenomena during hardening process of the 45 steel, PhD Thesis, Częstochowa 2005 (in Polish).

[6] D. P. Koistinen, R. E. Marburger, A general equation prrescribing the extent of the autenite-martensite transformation in pure iron-carbon alloys and plain carbon steels, Acta Mettalica, vol 7 (1959) 59-60

[7] K. J. Bathe, Finite element procedures in engineering analysis, Prentice-Hall, 1982.

[8] P. Bochev, Finite element methods based on least squares and modified variational principles. COM^{2}MAC Lecture Notes, Postech, Pohang, South Korea, 2001.

[9] T. J. R. Hughes, Recent progress in the development and understanding of SUPG methods with special reference to the compressible Euler and Navier-Stokes equations, International Journal for Numerical Methods in Fluids , vol. 7 (1987) 1261-1275.

[10] Z. Svoboda, The analysis the convective-conductive heat transfer in the building constructions, In: Proceedings of the 6th Building Simulation Conference, Kyoto (1999) 1: 329-335.

[11] A. Bokota, A. Kulawik, Three dimensional model of thermal phenomena determined by moving heat source, Archives of Foundry vol. 2, No. 4 (2002) 74–79 (in Polish).

[12] A. J. Chorin, Numerical solution of the Navier-Stokes equation, Math. Comput. (1968) 23:745-762.

[13] O. C. Zienkiewicz, R. Codina, A general algorithm for compressible and incompressible flow, Part I. The split characteristic based scheme, International Journal for Numerical Metods in Fluids (1995) 20:869-885.

[14] O. C. Zienkiewicz, R.L. Taylor, The finite element method, Volume 3: Fluid dynamics, Butterworth and Hienemann, 2000.

[15] J. Chessa, T. Belytschko, An extended finite element method for two-phase fluids, Journal of Applied Mechanics, vol. 70 (2003) 10-17.